IOPscience iopscience.iop.org

Home Search Collections Journals About Contact us My IOPscience

Plasma-made silicon nanograss and related nanostructures

This content has been downloaded from IOPscience. Please scroll down to see the full text.

2011 J. Phys. D: Appl. Phys. 44 174010

(http://iopscience.iop.org/0022-3727/44/17/174010)

View the table of contents for this issue, or go to the journal homepage for more

Download details:

IP Address: 140.113.38.11
This content was downloaded on 25/04/2014 at 00:02

Please note that terms and conditions apply.

J. Phys. D: Appl. Phys. **44** (2011) 174010 (6pp) doi:10.1088/0022-3727/44/17/174010

Plasma-made silicon nanograss and related nanostructures

Jiann Shieh[1,2], Srikanth Ravipati[3], Fu-Hsiang Ko[3] and Kostya (Ken) Ostrikov[2]

[1] Department of Materials Science and Engineering, National United University, Miaoli 36003, Taiwan
[2] Plasma Nanoscience Centre Australia (PNCA), CSIRO Materials Science and Engineering, Lindfield, New South Wales 2070, Australia
[3] Institute of Nanotechnology and Department of Materials Science and Engineering, National Chiao Tung University, Hsinchu 30010, Taiwan

E-mail: jshieh@nuu.edu.tw

Received 8 October 2010, in final form 29 December 2010
Published 14 April 2011
Online at stacks.iop.org/JPhysD/44/174010

Abstract
Plasma-made nanostructures show outstanding potential for applications in nanotechnology. This paper provides a concise overview on the progress of plasma-based synthesis and applications of silicon nanograss and related nanostructures. The materials described here include black silicon, Si nanotips produced using a self-masking technique as well as self-organized silicon nanocones and nanograss. The distinctive features of the Si nanograss, two-tier hierarchical and tilted nanograss structures are discussed. Specific applications based on the unique features of the silicon nanograss are also presented.

Introduction

Top-down and bottom-up nanofabrications are the two most common approaches for fabricating nanostructures. Bottom-up approaches rely on atomic and molecular building units (BUs) and can be used to produce nanoscale assemblies in the molecular size scale. In comparison, feature/structure size reduction in top-down approaches remains a major challenge. A combination of lithography and mask-assisted etching is a typical top-down technique. Semiconductor processes widely use plasma etching to produce micromorphology through a lithographic etching mask. In general, the mask size determines the feature size. Currently, the smallest feature size created by the state-of-the-art photolithography using water immersion technology is approximately 45 nm [1]. The wavelength of the exposure light source, high facility cost and low process throughput limit the achievable smallest feature size and thus represent a significant challenge.

On the other hand, plasma-based processes can be used to fabricate less regular nanostructures without any pattern delineation processes and have therefore, attracted major attention in recent years owing to their outstanding simplicity, efficacy and cost-efficiency. Recently, plasma-made nanostructures were extensively investigated both experimentally and theoretically [2–7]. Black silicon is a typical example of plasma-made lithography-free microstructures. In this process, nanoparticle masks that originate as a result of plasma-assisted polymerization or sputtering processes cannot be effectively controlled and compromise the process output. Producing nanoparticles in the plasma for masks extends the scope of the plasma-based nanofabrication. However, this approach does not solve persistent problems of size/position uniformity and down-scaling.

In the previous study, a hydrogen plasma-based approach was developed to create well-aligned silicon nanograss [8]. Compared with the black silicon and nanoparticle-assisted fabrications of nanostructures, the silicon nanograss had a smaller diameter (20 nm in base diameter) and a better size uniformity. However, many of the physical and chemical properties of the silicon nanograss remain unexplained. Here, plasma-based synthesis and applications of Si-based nanostructures including two-tier hierarchical nanotip structures, self-organized nanotips and mask-free nanograss are discussed. Furthermore, sample tilting and nanopillar supports are used to demonstrate the various possibilities on morphology control, which is one of the key issues in plasma-aided nanofabrication.

1. Black silicon

In 1924, Langmuir reported on dust generated in a plasma [9], which was not explored until the late 1970s–early 1980s.

 © 2011 IOP Publishing Ltd Printed in the UK & the USA

Thanks to rapid developments in the semiconductor industry, black silicon was discovered during the plasma etching of silicon wafers. The late 1970s marked the beginning of black silicon-related research, when Gittleman *et al* examined textured surfaces for antireflection applications [10]. Chlorine plasma was the etching and sputtering medium, and aluminium coated on the backside of the wafer was the dust source. The diameters and interparticle spacing of the captured dust particles were in the range 100–300 nm. Thereafter, numerous studies discussed black silicon formation mechanisms [11–15]. Initially, black silicon was an undesired by-product in semiconductor processing because of the accompanying dust contamination [16]. However, many applications, including photovoltaic solar cells [17], accelerometers [18], photodetectors [19] and surface with controlled wettability [20], benefit from the nanoscale morphology of black silicon and have recently attracted a continuously increasing interest.

In general, micromasks and anisotropic etching through the assistance of sidewall passivation on silicon pillars are essential to produce black silicon. The micromasks may originate from the products of plasma polymerization or sputtering of reactor walls and electrodes. On the other hand, reactive radicals generated through the surface- or gas-phase reactions can form the required passivation layer. To shed some light on the formation mechanism of hydrogen plasma-made silicon nanograss, the following section introduces basic aspects of the plasma-assisted etching of black silicon and related nanostructures.

1.1. Mask materials

Fabrication of plasma-made one-dimensional silicon, including black silicon, involves mask preparation. Without a regular lithographic pattern, most black silicon masks arise from sputtered debris. Several studies compared cathode materials and demonstrated that such masks consist of cathode materials. Pinto *et al* [21] and Gotza *et al* [13] compared aluminium/alumina and quartz cathodes and found that a rough morphology did not appear in quartz-covered cases. Schwartz *et al* [22] demonstrated that redeposition is the key mechanism of Al/Co mask formation on the surface.

Plasma polymerization is another chemical route for the mask formation. Smadi *et al* [16] investigated the chemistries of SF_6/Ar and CF_4/O_2/Ar discharges, and revealed that the masks were composed of the elements of the reaction gas and the substrate materials. Therefore, the masks are formed through redeposition of the particles released from the Si substrate as a result of sputtering and etching reactions. Similarly, in $HCl/O_2/BCl_3$ discharges, redeposited SiO_2 is believed to be the main mechanism of mask formation [14]. The diameter of silicon structures in the SiO_2-mask black silicon experiments is usually larger than a micrometre.

Most black silicon studies analyse mask composition and discuss the origin of any particular morphological features on the surface. The drawback of this method is a less controllable and predicable mask. To design particles for masks and to facilitate mask production for Si nanocone arrays, ion sputtering was applied [23]. Li *et al* [24] prepared carbon cone masks using Ar ion bombardment of the pre-deposited carbon film. Several studies examined various approaches to prepare nanomasks for hydrogen plasma-made nanostructures. For example, Hsu *et al* [25] applied SiH_4 and CH_4 to generate SiC nanoclusters as hard masks for etching silicon wafers, and obtained Si nanotips using Ar/H_2 plasma etching. She *et al* [26] generated SiC hard masks on silicon wafers using the CH_4/H_2 plasma and then applied the hydrogen plasma to etch the wafer. Furthermore, tungsten particles may work as an etching mask against hydrogen radicals to produce silicon surfaces with micro- and nano-textures [27].

1.2. Reactive species in the plasma

Halogen-based gases including fluorine and chlorine are commonly used as etching gases for black silicon production [7]. These gases contain a plethora of reactive radical species. Fluorine-based radicals react with a very large number of materials, and usually enable highly isotropic etching. Fluorine atoms have to be released from gas molecules to react with silicon. By adding oxygen gas to fluorine plasma, the concentration of atomic fluorine can be increased through oxidation of fluorine-based gas. The following process describes the extraction of fluorine atoms from a CF_4 precursor [28, 29]:

$$CF_4 + O \rightarrow COF_2 + 2F.$$

However, oxygen also reacts with fluorine atoms. Excessive amounts of oxygen can reduce the amount of atomic fluorine and can thus inhibit the fluorine etching process:

$$O_2 + F \rightarrow FO_2,$$

$$FO_2 + F \rightarrow F_2 + O_2.$$

Using CF_4+ 5% O_2 to treat wafers before etching can result in the self-formed masks [13]. In comparison, a gas mixture of CF_4(200 sccm) and O_2(100 sccm) gases was used for wafer conditioning before loading the wafers into the reaction chamber in Si nanograss studies [8]. Energy dispersive x-ray (EDX) analysis results showed that no traces of metal contamination were detected.

In addition, atomic hydrogen also scavenges F atoms to form HF:

$$H + F \rightarrow HF.$$

This may explain why hydrogen is usually considered as an inhibitor rather than an effective etching gas in fluorine and fluorocarbon plasmas.

However, atomic hydrogen alone can etch silicon or germanium to create nanograss and quantum dots. The ability to etch semiconductors owes to the reactions between hydrogen and semiconductor atoms leading to volatile covalent hydrides [30]. The etching rate of hydrogen plasma for Si is much higher (30×) than for SiO_2 [30]. Therefore, it is possible to selectively etch Si over silicon oxide using hydrogen plasma. Moreover, the incompletely removed (during the chamber conditioning) native oxide may act as a mask in the subsequent hydrogen selective etching, because of the lower etching rate of the oxide

layer compared with silicon. However, the contribution of the native oxide layer to hard masks is usually small because of their small (typically a few nanometres) thickness. In addition, the etch selectivity of SiO_2/Si also depends on the ion flux. Increasing the input ICP power will reduce the etch selectivity of SiO_2 over Si [31]. For nanograss production, a substrate bias was needed in hydrogen plasma etching to enhance the ion flux [8], which may reduce the SiO_2/Si selectively, also indicating that the native oxide mask does not play a major role for nanostructure evolution under large ion flux.

1.3. Sidewall passivation

Reaction products have to be volatile to enable effective reactive chemical etching. For example, volatile SiF_4 or Si_2F_6 can desorb from the substrate surface, because no bonds link them to the silicon surface. On the other hand, highly anisotropic etching requires effective passivation of the sidewalls. Examples of suitable non-volatile radical species include SiF_2 and SiF_3. Oxygen radicals also enhance etching anisotropy by combining with fluorine-based gases to passivate silicon surfaces with SiO_xF_y [12]. Less reactive Cl atoms may also adsorb on the sidewalls thus forming the required passivation layer to inhibit the isotropic etching. In $HCl/O_2/BCl_3$ plasma, sputtered silicon chlorides with high sticking coefficients can adsorb on sidewalls and produce silicon oxide passivation layers [14]. The major products in the reaction between the hydrogen plasma and silicon substrates are SiH_2 and SiH_3 [32], which are very reactive to re-adsorb on the silicon surface. The SiH_2 and SiH_3 radicals have large sticking coefficients and can thus effectively passivate Si surfaces.

2. Mask-free process

Many problems such as strong non-uniformity in the nanostructure height and size distributions are caused by the masks formed by the sputtered debris. In addition, black silicon is rarely observed in narrow trenches, because of the shadowing effect. This is why black Si-free areas near the pattern edges are frequently observed [14]. Therefore, the preferred plasma etching should ideally be mask-free. The absence of a mask obviously reduces the capability of selective etching. However, surface micro/nano-roughness enables the maskless etching. Indeed, CF_4/O_2 plasma-etched Si surfaces revealed a nanoscale roughness instead of the expected atomically smooth surface [33]. This nanomorphology may originate through redistribution of reactive etching species between the valleys and the hillocks on the surface. For example, CF_4 plasmas can create nanoscale columnar structures on silicon surfaces without a metal mask. Moreover, using plasma-polymerized fluorocarbon masks significantly improves the uniformity of the surface roughness [34]. In addition, the masks are not formed at low temperatures in SF_6/O_2 gas mixtures [35].

In addition to the plasma etching, self-organization in the plasma can lead to the formation of silicon nanocones and nanopyramids [36, 37]. Ar + H_2 plasma etching

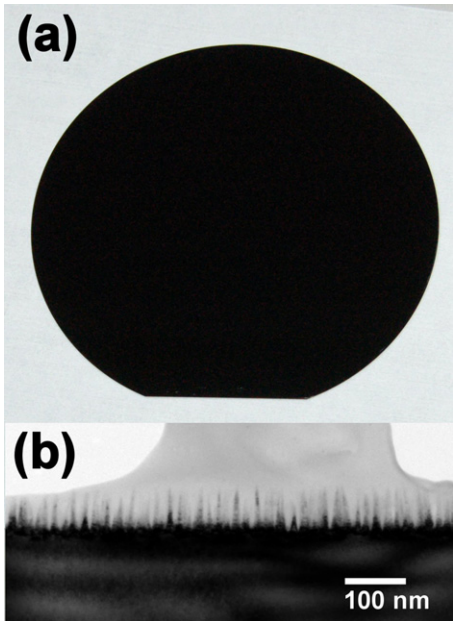

Figure 1. Photograph of a 6 inch silicon wafer decorated with silicon nanograss (*a*) and cross-sectional TEM image (*b*).

and sputtering effects release silicon atoms and Si-based radicals. The competition between the nanostructure growth processes (from reattachment of Si atoms, the deposition of SiH_x radicals and larger hydrogenated clusters) and surface termination by H atoms control nanostructure nucleation and growth. The total energy minimization principles determine the final nanostructure shape. Adding small amounts of hydrogen dramatically increases the energy flux in this self-organization-based process [38]. Hence, using a mixture of hydrogen, nitrogen and methane gases one can obtain silicon nanocones with a density of $10^8\,cm^{-2}$ through the plasma etching combined with silicon material redeposition [39]. The major difference between the etching and self-organization/redeposition scenarios could be the density and the aspect ratio of the nanostructures. In the growth and redeposition scenario, the small inter-nanostructure spacings available for BU delivery and the associated shadowing effect may substantially reduce the nanostructure density. However, for maskless etching, the density of the nanograss structures is expected to be higher.

Simultaneous high selectivity and anisotropy usually happen in narrow parameter spaces [36]. We have used ICP hydrogen plasma with a lower frequency bias to create silicon nanograss. In the absence of a mask, silicon nanograss is uniformly distributed over a large area. Figure 1 shows a cross-sectional transmission electron microscope (TEM) image and a picture of a 6 inch silicon wafer decorated with Si nanograss. Wafer processing in inductively coupled plasmas may provide such high uniformity. Another attractive feature of the nanograss is its high aspect ratio. The base diameter of each nanostructure is approximately 20 nm, which is much smaller compared with black silicon and SiC-cap nanotips [40]. The density of the nanograss can be as high as $10^{11}\,cm^{-2}$, which is almost 10 000 higher compared with typical black silicon [19]. In other words, there are 10^{13} nanotips formed

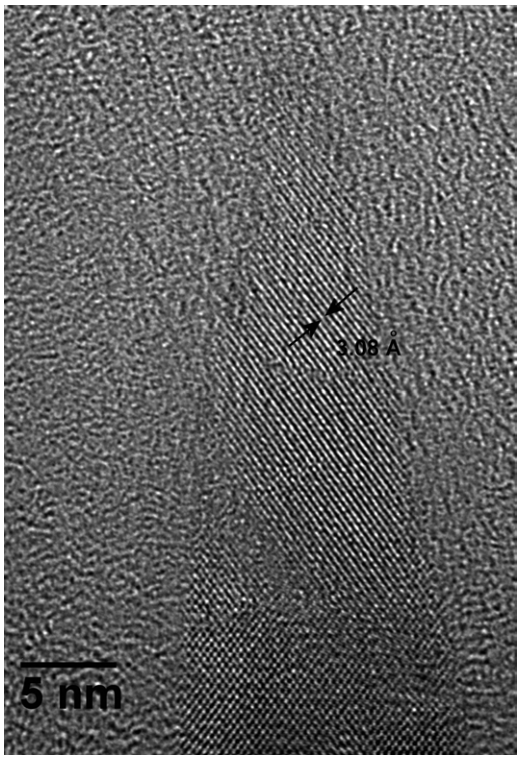

Figure 2. High-resolution TEM image of silicon nanograss.

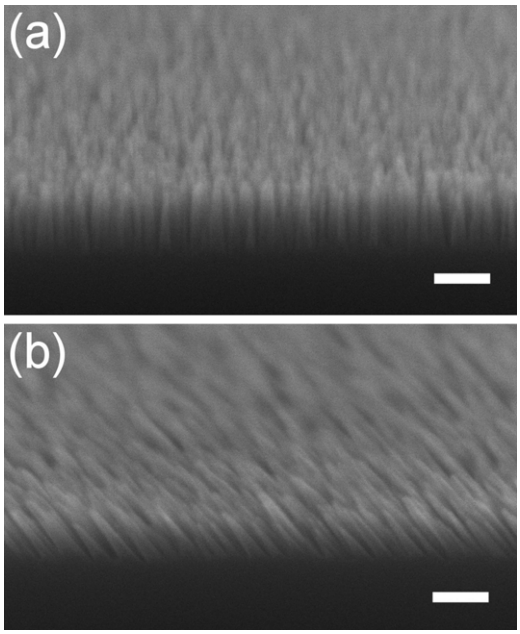

Figure 3. SEM images of vertically aligned Sinanograss at the sample centre (*a*) and tilted Si nanograss near the sample edge (*b*). (scale bars: 100 nm)

on the surface of a 6 inch silicon wafer. To enable effective antireflection, the pitch of individual nanostructures has to be less than the wavelength of light at normal incidence and less than a half of the wavelength at oblique incidence [41]. The pitch in the TEM image is approximately 20 nm. Therefore, the nanograss features are too small to be resolved by the incident light even in the UV spectral region. Hence, the diffraction effects can be neglected [42].

The uniformity in height of individual nanostructures also implies that nanoparticles are not generated in the gas phase during the hydrogen plasma etching. If the masks were formed by sputtered debris, then the mask deposition would be continuous and the resulting structures would be very non-uniform. A high-resolution TEM (HRTEM) image in figure 2 provides additional evidence on the absence of any mask. Indeed, the cap layer near the top of the structure has the same atomic ordering as Si (1 1 1).

3. Inclined nanograss

The development of silicon nanostructures with arbitrary angles with respect to the surface is interesting for applications as unidirectional wetting layers in microfluidic systems [43] and ultra-low refractive index films [44]. Recent studies using glancing- or oblique-angle deposition resulted in the creation of inclined nanostructures [45–47]. Random growth fluctuations may play a significant role in the evolution of a tilted columnar morphology by producing a shadow region to inhibit the incoming vapour flux. Another route to inclined one-dimensional nanostructures involves the plasma process. Several studies revealed that the alignment of carbon nanotubes (CNTs), determined by the direction of the electric field lines, deviated from the direction normal to the substrate near the sample edge due to edge effects in the plasma sheath [48–50]. Similar effects were reported for amorphous silicon [51] and diamond nanocones [52].

The hydrogen plasma etching process was extended to tilted nanostructures here. When the substrate was tilted at an angle of 30°, the morphology of the silicon nanograss changed near the sample edge (figure 3(*a*)). However, the nanograss structures far away from the edge (several millimetres) was still perpendicular to the substrate (figure 3(*b*)), which indicates that the plasma sheath profile followed the substrate shape, and that the plasma etching near the sample edge can be used to fabricate uniformly tilted Si nanograss.

4. Nanograss on nanopillars

The size of one-dimensional silicon nanostructures fabricated by the plasma etching was usually larger than 100 nm [19, 23, 39, 40], whereas the size of the silicon nanograss was much smaller. This can be due to slower etching rates of hydrogen ions/radicals and the absence of any foreign mask materials. The properties of the silicon nanograss can be exploited to enhance the stability of superhydrophobic surfaces, because of the ultra-fine nanoscale surface morphology. Superhydrophobicity is defined as a hard-to-wet surface with large water-droplet contact angle (exceeding 150°) and small sliding angle (e.g. less than 10°) [53]. However, sticky superhydrophobicity (contact angle $>150°$) has been found in some rough surfaces [54–56]. For nanograss alone, the superhydrophobicity is sticky, and the sliding angle can be larger than 60°. After introducing nanopillar as the underlayer to reduce the nanograss density, the superhydrophobicity becomes slippery, that is, the sliding

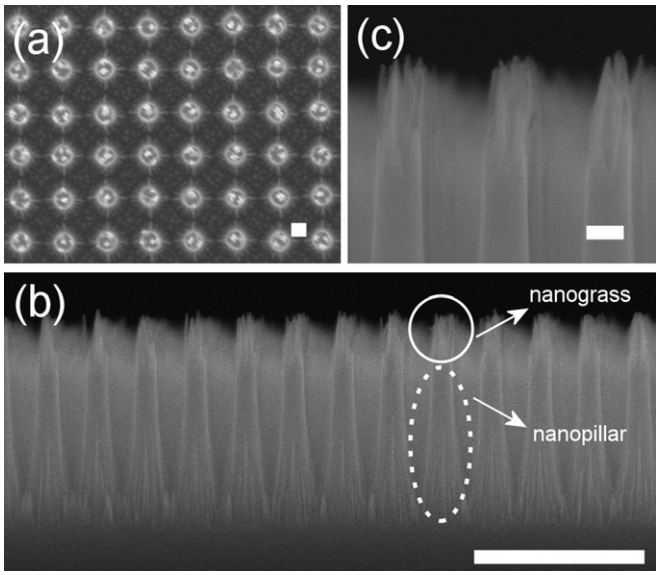

Figure 4. SEM images of the self-organized silicon nanograss on pre-fabricated nanopillars. (*a*) Top-view. (*b*) Cross-sectional view. (*c*) High-magnification cross-sectional view. The scale bars correspond to 100 nm (*a*), (*c*) and 1 μm (*b*).

angle is close to zero degrees [57]. Figure 4 shows SEM images of Si nanograss grown on a Si nanopillar. The nanopillar structures were fabricated using electron beam lithography. The nanopillars significantly improve the superhydrophobic stability compared with bare micropillars [58]. To enhance the superhydrophobic response even further, even smaller nanostructures on the nanopillar top surface are required, which is a big challenge for nanofabrication based on optical and e-beam lithography. If nanoparticles are generated as hard masks, it is difficult to ascertain that every nanoparticle sits in the desired position on the small top surface. Etching in hydrogen plasmas proceeds at an atomic scale without any mask assistance; in this way one can obtain the desired hierarchical nanoscale two-tier morphology. The surface can sustain a static pressure of 234 Pa without losing the nearly perfect superhydrophobicity, even when the air fraction exceeds 99.98% [57].

5. Applications

The ability to fabricate two-tier hierarchical self-organized nanostructures offers additional benefits in various applications. For example, it has been reported that the field emission performance of the two-tier nanostructures can be even better compared with nanopillar and nanograss structures [59]. It was also suggested that this effect may be attributed to the adjustment of electrostatic screening effects by the small nanostructures on top of the nanopillars.

In another application, thermal nanoimprinting was used to transfer the nanograss into cyclic olefin copolymer (COC) plastic substrates [60]. In this way, sub-20 nm nanotip patterns and nanopore arrays on plastic were realized. This led to the two significant effects. First, there was a significant increase in optical transparency. Second, the native contact angle increased to the superhydrophobic value; this was achieved without any intentional surface functionalization of the plastic surface.

Recently, Chang *et al* [61] used Si nanograss as a high-specific-area antireflective material to enhance visible photoluminescence intensity of ZnO layers. ZnO/nanograss heterostructure exhibited a much brighter emission than a ZnO thin film without silicon nanograss. Furthermore, Otto *et al* [62] used black silicon as an underlayer to reduce the reflectivity of conformal transparent conducting oxide ZnO : Al layers. This effect can significantly improve the performance of heterojunction photovoltaicsolar cells in the future.

6. Summary

In this paper, we have discussed the progress achieved in the area of plasma-made Si nanograss and related nanostructures. In particular, we have introduced representative chemical reactions involved in the formation of silicon nanograss in hydrogen plasmas. During hydrogen plasma etching, plasma–surface interactions lead to the surface roughening. Strong material removal from the valley eventually results in nanograss formation. Surface passivation of the sidewalls of the nanograss by adhering radicals such as SiH_2 and SiH_3 also contributes to the significant etching anisotropy. A negligible amount of mask material detected via EDS and HRTEM analyses demonstrates that masks are absent in the hydrogen plasma etching, which in turn results in very high surface density ($\sim 10^{11}$ cm^{-2}) of the silicon nanograss.

To demonstrate the power of hydrogen plasma etching, novel nanostructures including tilted and two-tier nanograss structures have also been presented. Although the mechanism beyond this highly anisotropic hydrogen plasma etching still awaits further detailed analysis, the advantages of high-uniformity and high aspect ratios enable several important applications. One can thus expect that hydrogen-based plasma etching can also be used for the fabrication of non-silicon nanograss with presently unknown properties and applications. This approach may offer viable practical alternatives to several conventional ways to produce semiconductor quasi-one-dimensional nanostructures [63–65].

Acknowledgments

The authors thank C C Cheng, C C Hong, Y C Chen, F J Hou, H M Chen, S P Yang, P Huang, I Levchenko and other collaborators for their contributions to the area of Si nanograss research. Financial support is acknowledged from the National Science Council of Taiwan (NSC 99-2221-E-492-003). This work was partially supported by the CSIRO's OCE Science Leadership program.

References

[1] The International Technology Roadmap for Semiconductors(ITRS) 2009 edition. Available from http://www.itrs.net
[2] Ostrikov K 2005 *Rev. Mod. Phys.* **77** 489

[3] Ostrikov K and Murphy A B 2007 *J. Phys. D: Appl. Phys.* **40** 2223
[4] Chattopadhyay S, Chen L C and Chen K H 2006 *Crit. Rev. Solid State Mater. Sci.* **31** 15
[5] Chattopadhyay S, Ganguly A, Chen K H and Chen L C 2009 *Crit. Rev. Solid State Mater. Sci.* **34** 224
[6] Chattopadhyay S, Huang Y F, Jen Y J, Ganguly A, Chen K H and Chen L C 2010 *Mater. Sci. Eng.* R **69** 1
[7] Zheng J, Yang R, Xie L, Qu J, Liu Y and Li X 2010 *Adv. Mater.* **22** 1451
[8] Yang M C, Shieh J, Hsu C C and Cheng T C 2005 *Electrochem. Solid State Lett.* **8** C131
[9] Langmuir I, Found G and Dittmer A F 1924 *Science* **60** 392
[10] Gittleman J I, Sichel E K, Lehmann H W and Widmer R 1979 *Appl. Phys. Lett.* **35** 742
[11] Chow T P, Maciel P A and Fanelli G M 1987 *J Electrochem. Soc.* **134** 1281
[12] Jansen H, de Boer M, Legtenberg R and Elwenspoek M 1995 *J. Micromech. Microeng.* **5** 115
[13] Gotza M, Saint-Cricq B, Dutoit M and Jouneau P H 1995 *Microelectron. Eng.* **27** 129
[14] Oehrlein G S, Rembetski J F and Payne E H 1990 *J. Vac. Sci. Technol.* B **8** 1199
[15] Legtenberg R, Jansen H, de Boer M and Elwenspoek M 1995 *J. Electrochem. Soc.* **142** 2020
[16] Smadi M M, Kong G Y, Carlile R N and Beck S E 1992 *J. Electrochem. Soc.* **139** 3356
[17] Yoo J S, Parm I O, Gangopadhyay U, Kim K, Dhungel S K, Mangalaraj D and Yi J 2006 *Sol. Energy Mater. Solar Cells* **90** 3085
[18] Mehran M, Mohajerzadeh S, Sanaee Z and Abdi Y 2010 *Appl. Phys. Lett.* **96** 203101
[19] Huang Z, Carey J E, Liu M, Guo X, Mazur E and Campbell J C 2006 *Appl. Phys. Lett.* **89** 033506
[20] Dorrer C and Rühe J 2008 *Adv. Mater.* **20** 159
[21] Pinto R, Ramanathan K V and Babu R S 1987 *J. Electrochem. Soc.* **134** 165
[22] Schwartz G C, Rothman L B and Schopen T J 1979 *J. Electrochem. Soc.* **126** 464
[23] Shang N G, Meng F Y, Au F C K, Li Q, Lee C S, Bello I and Lee S T 2002 *Adv. Mater.* **14** 1308
[24] Li Q, Ni Z, Yang S, Gong J, Zhu D and Zhu Z 2008 *Nucl. Instrum. Methods Phys. Res.* B **266** 197
[25] Hsu C H, Lo H C, Chen C F, Wu C T, Hwang J S, Das D, Tsai J, Chen L C and Chen K H 2004 *Nano Lett.* **4** 471
[26] She J C, Deng S Z, Xu N S, Yao R H and Chen J 2006 *Appl. Phys. Lett.* **88** 013112
[27] Nagayoshi H, Konno K, Nishimura S and Terashima K 2005 *Japan. J. Appl. Phys.* **44** 7839
[28] Pearton S J and Norton D P 2005 *Plasma Process. Polym.* **2** 16
[29] Van Toosmalen A J 1984 *Vacuum* **34** 429
[30] Chang R P H, Chang C C and Darack S 1982 *J. Vac. Sci. Technol.* **20** 45
[31] Zhong X X, Tam E, Huang X Z, Colpo P, Rossi F and Ostrikov K 2010 *Phys. Plasmas* **17** 094501
[32] Sun Y, Nishitani R and Miyasato T 1994 *Japan. J. Appl. Phys.* **33** L1117
[33] Zhao Y P, Drotar J T, Wang G C and Lu T M 1999 *Phys. Rev. Lett.* **82** 4882
[34] Gharghi M and Sivoththaman S 2006 *J. Vac. Sci. Technol.* A **24** 723
[35] Dussart R, Mellhaoui X, Tillocher T, Lefaucheux P, Volatier M, Socquet-Clerc C, Brault P and Ranson P 2005 *J. Phys. D: Appl. Phys.* **38** 3395
[36] Xu S, Levchenko I, Huang S Y and Ostrikov K 2009 *Appl. Phys. Lett.* **95** 111505
[37] Levchenko I, Huang S Y, Ostrikov K and Xu S 2010 *Nanotechnology* **21** 025605
[38] Wolter M, Levchenko I, Kersten H and Ostrikov K 2010 *Appl. Phys. Lett.* **96** 133105
[39] Bai X D, Xu Z, Liu S and Wang E G 2005 *Sci. Technol. Adv. Mater.* **6** 804
[40] Huang Y F *et al* 2007 *Nature Nanotechnol.* **2** 770
[41] Li Y, Zhang J and Yang B 2010 *Nano Today* **5** 117
[42] Shieh J, Lin C H and Yang M C 2007 *J Phys. D: Appl. Phys.* **40** 2242
[43] Chu K H, Xiao R and Wang E N 2010 *Nature Mater.* **9** 413
[44] Xi J Q, Schubert M F, Kim J K, Schubert E F, Chen M, Lin S Y, Liu W and Smart J A 2007 *Nature Photon.* **1** 176
[45] Ma Y, Liu F, Zhu M, Liu J, Wang H, Yang Y and Li Y 2009 *Nanotechnology* **20** 275201
[46] Xi J Q, Kim J K, Schubert E F, Ye D, Lu T M and Lin S Y 2006 *Opt. Lett.* **31** 601
[47] Hawkeye M W and Brett M J 2007 *J. Vac. Sci. Technol.* A **25** 1317
[48] Merkulov V I, Melechko A V, Guillorn M A, Simpson M L, Lowndes D H, Whealton J H and Raridon R J 2002 *Appl. Phys. Lett.* **80** 4816
[49] Yang Q, Xiao C, Chen W, Singh A K, Asai T and Hirose A 2003 *Diamond Relat. Mater.* **12** 1482
[50] Lin C C, Liu I C, Yen J H and Hon M H 2004 *Nanotechnology* **15** 176
[51] Chaisitsak S 2007 *Mater. Sci. Eng.* B **137** 205
[52] Yang Q, Hamilton T, Xiao C, Hirose A and Moewes A 2006 *Thin Solid Films* **494** 110
[53] Feng L, Li S, Li Y, Li H, Zhang L, Zhai J, Song Y, Liu B, Jiang L and Zhu D 2002 *Adv. Mater.* **14** 1857
[54] Jin M, Feng X, Feng L, Sun T, Zhai J and Jiang L 2005 *Adv. Mater.* **17** 1977
[55] Guo Z G and Liu W M 2007 *Appl. Phys. Lett.* **90** 223111
[56] Bhushan B and Nosonovsky M 2010 *Phil. Trans. R. Soc.* A **368** 4713
[57] Shieh J, Hou F J, Chen Y C, Chen H M, Yang S P, Cheng C C and Chen H L 2010 *Adv. Mater.* **22** 597
[58] Extrand C W 2004 *Langmuir* **20** 5013
[59] Ravipati S, Kuo C J, Shieh J, Chou C T and Ko F H 2010 *Microelectron. Reliab.* **50** 1973
[60] Hong C C, Huang P and Shieh J 2010 *Macromolecules* **43** 7722
[61] Chang Y M, Jian S R, Lee H Y, Lin C M and Juang J Y 2010 *Nanotechnology* **21** 385705
[62] Otto M, Kroll M, Käsebier T, Lee S M, Putkonen M, Salzer R, Miclea P T and Wehrspohn R B 2010 *Adv. Mater.* **22** 5035
[63] Cvelbar U, Ostrikov K, Drenik A and Mozetic M 2008 *Appl. Phys. Lett.* **92** 133505
[64] Cvelbar U, Chen Z Q, Sunkara K and Mozetic M 2008 *Small* **4** 1610
[65] Meyyappan M and Sunkara M K 2010 *Inorganic Nanowires: Applications, Properties, and Characterization* (Boca Raton, FL: CRC press)